PCCP

Entropic selectivity in air separation via a bilayer nanoporous graphene membrane

Journal:	*Physical Chemistry Chemical Physics*
Manuscript ID	CP-ART-05-2019-002670.R1
Article Type:	Paper
Date Submitted by the Author:	12-Jun-2019
Complete List of Authors:	Wang, Song; University of California, Riverside, Department of Chemistry Dai, Sheng; Oak Ridge National Laboratory, Jiang, De-en; University of California, Riverside, Department of Chemistry

Entropic selectivity in air separation via a bilayer nanoporous graphene membrane

Song Wang,[a] Sheng Dai,[b,c] and De-en Jiang*[a]

[a]*Department of Chemistry, University of California, Riverside, California 92521, United States*

[b]*Chemical Sciences Division, Oak Ridge National Laboratory, Oak Ridge, Tennessee 37831, United States*

[c]*Department of Chemistry, The University of Tennessee, Knoxville, Tennessee 37996, United States*

*Corresponding author. Email: djiang@ucr.edu

ABSTRACT: Membranes are an energy-efficient technology for air separation, but it is difficult to control the pore size to separate N_2 and O_2 due to their similar kinetic diameters. Here we demonstrate from molecular dynamics simulations that a bilayer nanoporous graphene membrane with continuously tunable pore sizes by the offset between the two graphene layers can achieve O_2/N_2 selectivity up to 26 with a permeance over 10^5 GPU. We find that the entropic selectivity is the main reason behind the high selectivity via the tumbling movement of the skinnier and shorter O_2 molecules entering and passing through the elliptic-cylinder-shaped nanopore of the bilayer membrane. Such motion is absent in the single-layer graphene membrane with a similar-sized and similar-shaped pore which yields an O_2/N_2 selectivity of only 6 via molecular sieving alone. Hence the bilayer nanoporous graphene membrane provides a novel way to enhance entropic selectivity for gas separation via control of both the pore size and the 3D pore shape.

1. INTRODUCTION

Pure oxygen is widely used in medical, chemical, and material applications. Pure nitrogen is also important as a feedstock in ammonia synthesis, an inert atmosphere, or a coolant. Hence air separation is paramount for many industrial and medical uses. Conventionally, large-scale oxygen/nitrogen production by air separation is performed by the energy-intensive cryogenic distillation process.[1-3] For small to medium scales, other technologies such as pressure-swing-adsorption and membranes are also employed.[4-8]

Membrane technologies can provide a more energy-efficient alternative for air separation.[4, 8] An increasing number of membrane materials have been synthesized, such as polymers, zeolites, inorganic ceramic materials, carbon molecular sieves (CMS), and metal-organic frameworks (MOFs).[9-14] There is a well-known trade-off between membrane selectivity and membrane permeability, called the Robeson upper bound.[10, 15, 16] To surpass the upper bound, various approaches have been suggested for next-generation molecularly selective synthetic membranes, for example, using advanced semi-rigid polymers, hybrid materials, or scalable molecular sieves.[14]

One-atom-thin membranes such as porous graphene offers an attractive feature of ultra-high permeance and selectivity for gas separations based on molecule sieving.[17-22] However, due to the similar kinetic diameters of N_2 (3.64 Å) and O_2 (3.46 Å) and the discontinuously varying pore size on the graphene sheet, high O_2/N_2 selectivity is hard to achieve via the monolayer nanoporous graphene membranes. It is well known that the kinetic selectivity favors O_2 over N_2 in carbon molecular sieves via the ultramicropore windows.[10] This selectivity has been attributed to an entropic factor that favors a smaller molecule at the transition state, while the diffusion motion of the larger molecule is hindered.

Given the increasing interest in graphene and other 2D membranes for molecular and ion transport,[23, 24] one wonders if the entropic selectivity of O_2/N_2 can be achieved by a nanoporous graphene membrane. To address this question, we perform classical molecular dynamics simulations and show that high nanoporous entropic selectivity of O_2/N_2 can be achieved via O_2 tumbling through a bilayer nanoporous graphene membrane. Below we first explain our simulation

methods and then show our membrane design and performance. This is followed by the explanation and analysis of the selectivity mechanism and then the implications of our results and main conclusions.

2. COMPUTATIONAL METHOD

Classical molecular dynamics (CMD) simulations were performed with the LAMMPS package[25] in the canonical (NVT) ensemble at 300 K via the Nose-Hoover thermostat.[26, 27] The simulation box of $10\times10\times20$ nm^3 with periodic boundaries in the *xy* directions was divided into two chambers along the *z* direction by the bilayer nanoporous graphene membrane (Fig. S1, ESI): the feed side was pressurized at 10 bar, while the permeate side was vacuum initially. Single-component or pure-gas permeance was simulated; the feed pressure was initialized by randomly placing a certain number of pure gas molecules in the feed side to yield a pressure of 10 bar according to the ideal-gas law. The top and the bottom of the bi-chamber system were bound by two impermeable fixed walls. NVT simulations were performed, so the feed side pressure would decrease while the permeate side pressure would increase, until equilibrium is reached when both chambers have the same pressure. The duration of each simulation was 10 ns; the number of molecules in the permeate side was counted every 10 ps, to monitor the gas permeation across the membrane over time.

The bilayer nanoporous graphene membrane was fixed during the simulations. This is a good approximation because of the rather high tensile strength of graphene. In addition, when used in practice the graphene membrane is expected to be supported on a mechanically strong and more porous substrate, so the out-of-the-plane motion of the graphene layer should also be minimal. To further confirm that the vibrational motion of the atoms in the membrane has negligible effect on the gas permeance, we have simulated and compared gas permeance through frozen and flexible graphene membranes. As shown in Fig. S2, the impact of allowing the graphene membrane to be flexible is indeed small on the gas permeance, so in all our simulations the membrane was frozen.

The force-field parameters for the membrane (consisting of carbon and hydrogen atoms only) were given in ESI. For O_2 and N_2, three-site models were adopted.[28] O_2 and N_2 molecules were rigid and were not allowed to vibrate during our simulations. This assumption is reasonable given the very high vibrational temperatures of the two molecules: 3521 K for N_2 and 2256 K for O_2; our calculated mean amplitudes of vibration at 300 K are 0.0367 Å for O_2 and 0.0314 Å for N_2 (see ESI), which are negligible compared with their kinetic diameters (3.46 Å for O_2 and 3.64 Å for N_2). The LJ potential parameters were calculated by using Lorentz-Berthelot Combining Rules. The cutoff distance for Lennard-Jones and Coulombic potential was 12 Å. The long ranged electrostatic interaction was calculated using the PPPM method with a k-space slab correction.[29-31] Free-energy profiles were calculated via the umbrella sampling method implemented in the PLUMED tool.[32] The weighted histogram analysis method (WHAM) was applied to reconstruct the free energy profile.[33]

3. RESULTS AND DISCUSSION

3.1. Membrane setup

Bilayer nanoporous graphene membranes provide an effective way to continuously tune the pore size at sub-angstrom resolution via the offset between the two one-atom-thin membranes.[34] It also offers a knob to control the diffusion path through the bilayer membrane. Fig. 1a shows the single-layer porous graphene used to build the bilayer. It has an all-hydrogen-terminated pore of 5.7 Å in size which is much greater than the sizes of O_2 and N_2 (Fig. 1d). So the single-layer membrane would not have any O_2/N_2 selectivity (that is, it is close to 1). The bilayer membrane is then constructed with an interlayer spacing of 3.4 Å (similar that in graphite) between the two porous single-layer graphene membranes (Fig. 1b), so there is no adsorption between the two layers (the accessible pore size in between the layers is hence zero). The offset (Fig. 1c) can be tuned to control the effective pore size of the bilayer membrane for gas permeation.

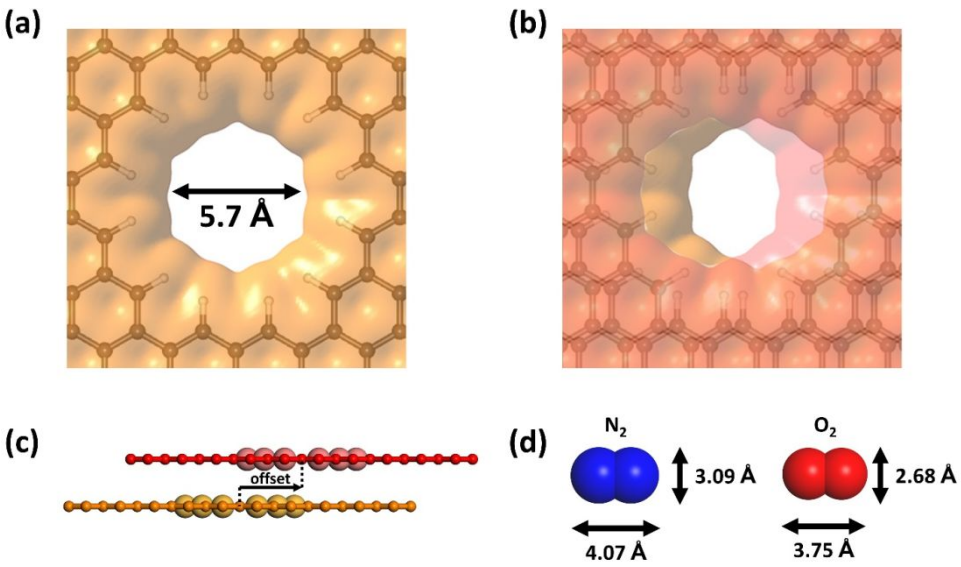

Fig. 1. (a) Single-layer graphene pore; (b) bilayer nanoporous graphene membrane; (c) side view of the bilayer nanoporous graphene membrane with an offset of the two pore centers (the larger spheres indicate the pore rims); (d) molecular sizes of nitrogen and oxygen. In (a) and (b), the pore shapes and sizes are estimated by the isosurfaces of electron density at 0.0004 e/a_0^3 where a_0 is the Bohr radius.

3.2. O_2/N_2 permeation through the bilayer membrane

Classical molecular dynamics simulations were performed to follow the trajectories of the gas molecules. Fig. 2 shows the number of gas molecules (N_2 or O_2) permeating through the bilayer membrane with time for different effective pore sizes. The effective size is determined by a simple analytical relationship with the offset (Fig. S1; ESI). When the effective pore size is 3.60 Å (Fig. 2a), both of N_2 and O_2 have high permeances. When the effective pore size decreases to 3.50 Å (Fig. 2b), N_2 permeance is significantly reduced while O_2 permeance decrease only slightly, indicating an increase in O_2/N_2 selectivity. When the effective pore size further decreases to 3.45 Å (Fig. 2c), N_2 permeance is greatly reduced, because now the pore size is much less than the N_2 kinetic dimeter (3.64 Å) but still comparable to O_2 kinetic diameter (3.46 Å). When the effective pore size further decreases to 3.40 Å (Fig. 2d), now O_2 permeance is also greatly reduced. Fig. 2 suggests that an effective pore size of 3.45 Å would be optimal for O_2/N_2 selectivity and O_2 permeance.

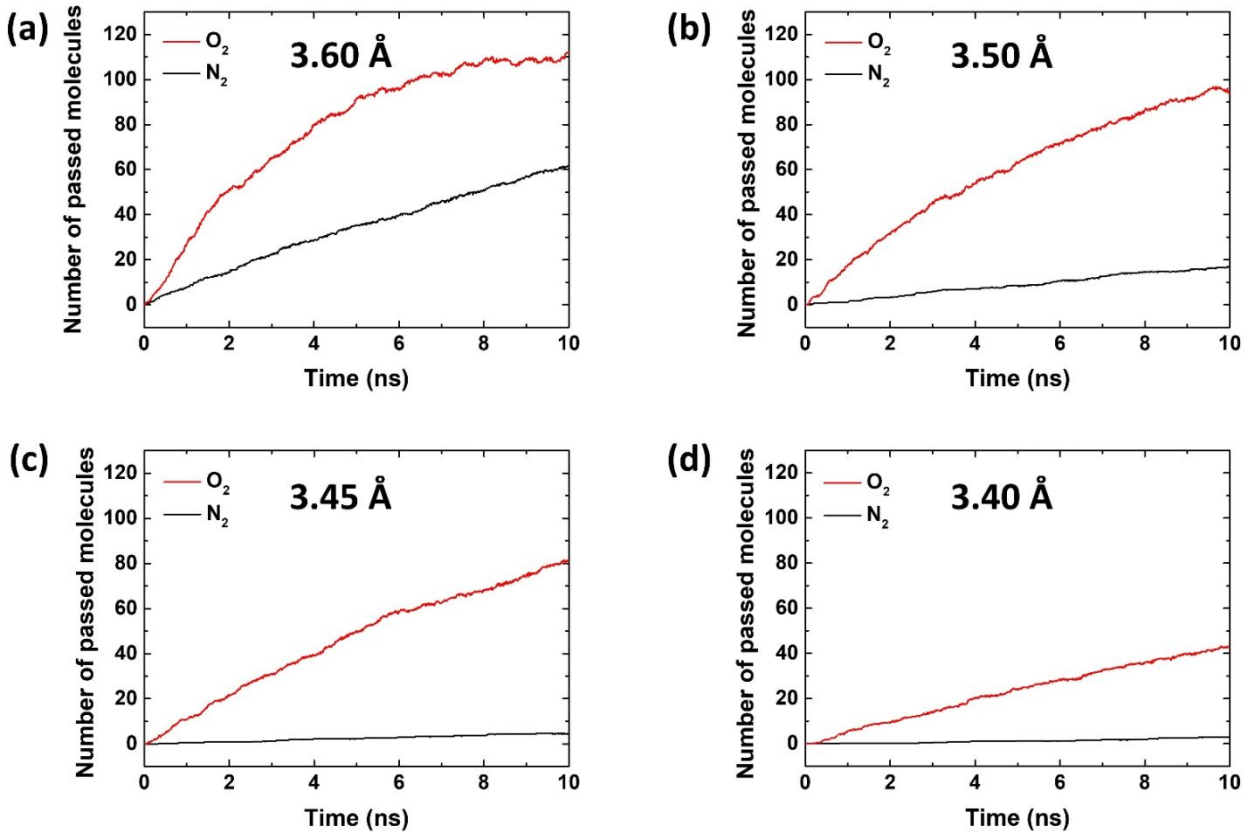

Fig. 2. The numbers of gas molecules passed through the bilayer nanoporous graphene membranes with different effective pore sizes: (a) 3.60 Å; (b) 3.50 Å; (c) 3.45 Å; (d) 3.40 Å.

3.3. O_2/N_2 selectivity

To analyze the relationship between the O_2/N_2 selectivity and the effective pore size, we first fit the curves in Fig. 2 via an exponential model, $y = a * (1 - e^{-\lambda t})$,[35] to obtain the fitting parameter a and λ whose product is proportional to the permeance. Fig. 3 shows how O_2 and N_2 permeances and O_2/N_2 permselectivity vary with the effective pore size. One can see that the effective pore size of 3.45 Å affords the highest selectivity of 25.6, while the O_2 permeance is at 5 × 10^5 GPU (gas permeation unit). For comparison, carbon molecular sieve (CMS) membranes show O_2/N_2 selectivity of 8 – 25.[13, 36] So the bilayer nanoporous graphene membrane with the optimal effective pore size rivals the best CMS membranes in terms of O_2/N_2 selectivity.

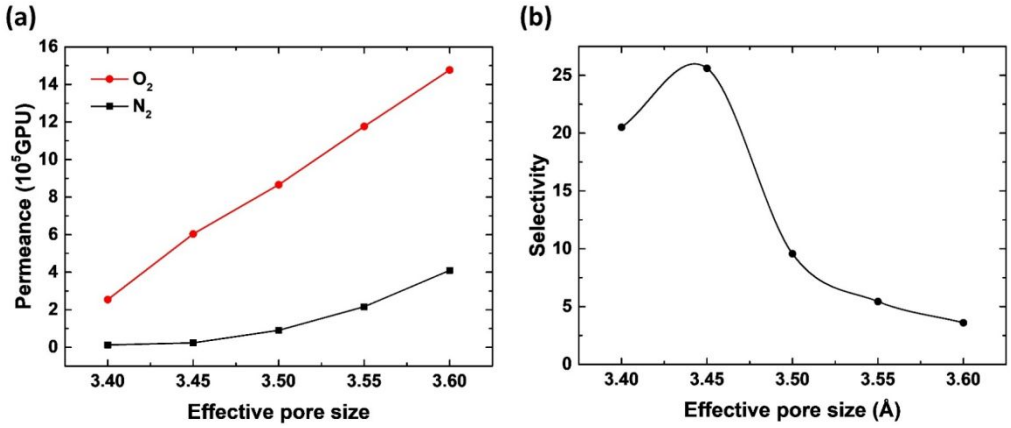

Fig. 3. O_2 and N_2 permeances (a) and O_2/N_2 permselectivity (b) of the bilayer nanoporous graphene membranes with different effective pore sizes.

3.4 Mechanism of O_2/N_2 separation

For ultrathin membranes such as porous graphene, gas permeation usually consists of two main steps: adsorption on the surface of the feed side and diffusion across the membrane.[14, 37] To determine which step dictates the selectivity, we analyze them separately. Fig. 4 shows that the coverages of N_2 and O_2 on the feed side with time for the bilayer membrane with the optimal effective pore size of 3.45 Å. One can see that both gases reach their maximum coverages very quickly (< 1 ns). Then O_2 coverage slightly decreases, while N_2 coverage fluctuates. After 4 ns, O_2 and N_2 coverages are close to each other and in fact N_2 coverage is slightly higher, so the adsorption selectivity is close 1, which means that O_2/N_2 permselectivity is dictated by the diffusion process.

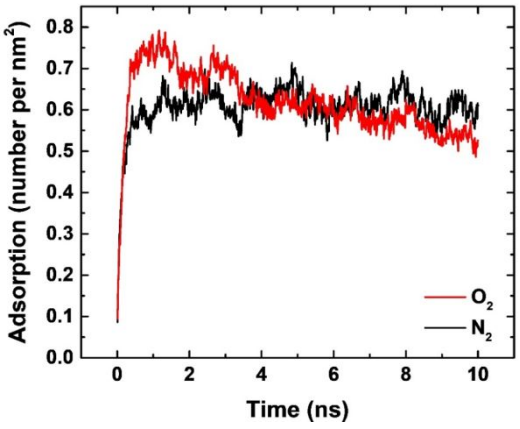

Fig. 4. Adsorption amount on the feed site of the bilayer nanoporous graphene membrane (effective pore size at 3.45 Å) with time.

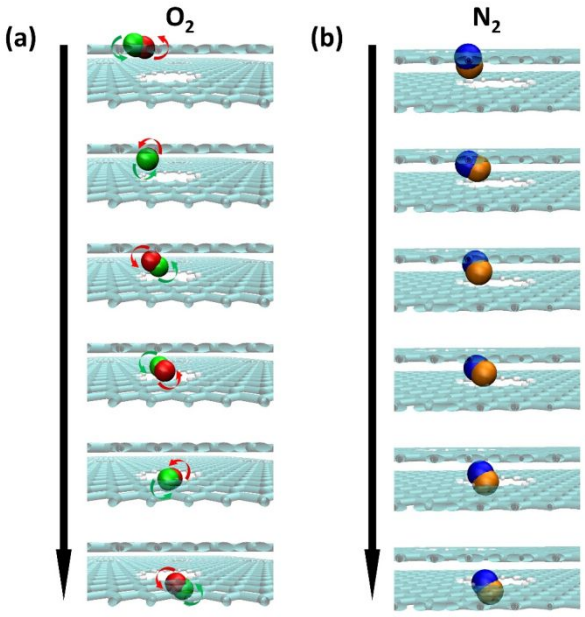

Fig. 5. Snapshots of (a) O_2 and (b) N_2 passing through bilayer nanoporous graphene membrane with effective pore size of 3.45 Å.

To understand how the bilayer membrane modulates the diffusion process and hence yields the high O_2/N_2 selectivity, we tracked and analyzed the motions of O_2 and N_2 molecules passing through the membrane. As shown in Fig. 5 (also see movies in ESI), the skinnier and shorter O_2 molecule tumbles through the elliptical-shaped nanopore (Fig. 5a), while the longer and fatter N_2 molecule wiggles through the nanopore with the rotational degrees of freedom hindered (Fig. 5b). Hence the unique elliptical-shaped nanopore in the bilayer graphene greatly facilitates the tumbling of O_2.

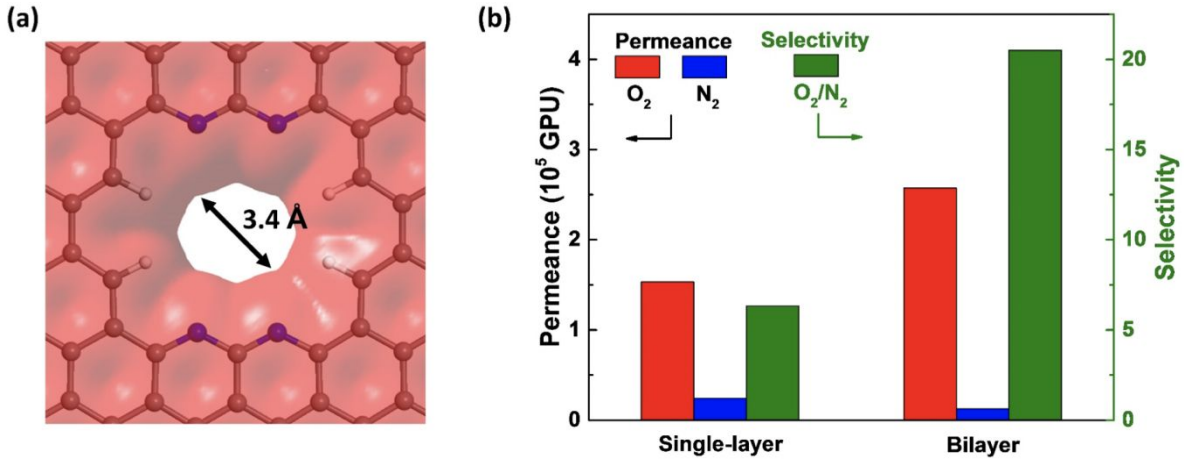

Fig. 6. (a) A single-layer porous graphene membrane with a pore of an elliptic shape and an average pore size of 3.4 Å. (b) Comparison of O_2 and N_2 permeances as well as O_2/N_2 selectivity between a single-layer graphene with a pore size of 3.4 Å and the bilayer graphene membrane with an effective pore size of 3.4 Å.

To further show that the distinct difference of this bilayer-graphene nanopore from the single-layer graphene pore, we also simulated O_2/N_2 separation through a single-layer graphene pore with an elliptic shape and an average pore size of 3.4 Å (Fig. 6a). As shown in Fig. 6b, in comparison with the performances of the bilayer graphene membrane of the similar pore size, the O_2 permeance becomes lower while the N_2 permeance becomes higher through the single-layer membrane, leading to a lower O_2/N_2 selectivity of 7. Further analysis of the trajectories confirmed that there is no tumbling motion for either O_2 or N_2 in passing through the single-layer membrane. In other words, the size-sieving effect of the single-layer membrane achieves O_2/N_2 selectivity of 7, while the additional entropic effect via the tumbling of the O_2 molecule through the bilayer membrane increases the selectivity by two times.

Figs. 5 and 6 clearly indicate that it is the entropic effect that yields the high O_2/N_2 selectivity through the bilayer graphene membrane, due to the extra unconstrained rotational degrees of freedom that O_2 enjoys at the transition state. To quantify this entropic difference, we applied the umbrella sampling method to determine the free-energy profiles of permeation for N_2 and O_2 through the bilayer membrane (Fig. 6). The two porous graphene layers are at z = ±1.7 Å. For

both O_2 and N_2, the transition state is at the middle of the bilayer (z = 0), with the free energy barrier of 5.08 kcal/mol for N_2 permeation and 3.18 kcal/mol for O_2. If we apply the transition-state theory, the free-energy-barrier difference would yield an O_2/N_2 selectivity of 24.5, which is consistent with the selectivity of 25.6 from CMD simulations. The 1.9 kcal/mol difference between N_2 and O_2 at the transition state should mainly result from the entropy contribution, since a simple estimate of the entropy difference from the partition functions would yield a contribution to the free energy at 1.7 kcal/mol at room temperature (see ESI).

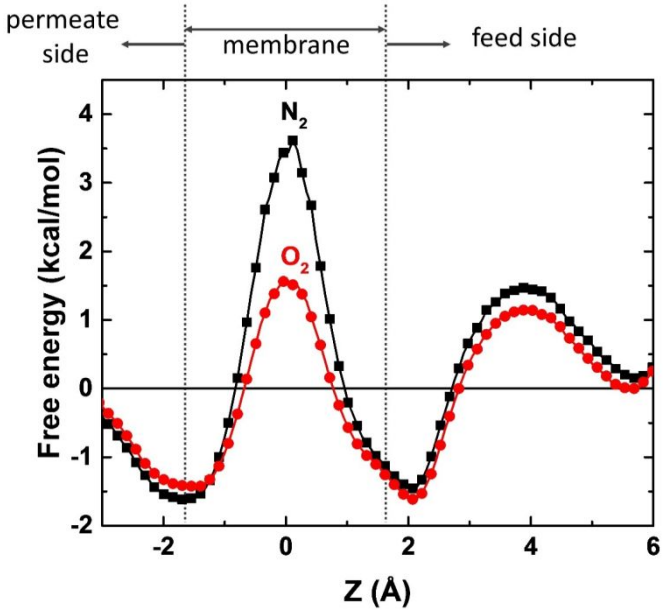

Fig. 7. Free energy profiles of gas-permeation through the bilayer nanoporous graphene membrane (effective pore size at 3.45 Å) for N_2 and O_2.

To further show the favorable entropic selectivity in the bilayer graphene membrane, we simulated the temperature effect on the selectivity whereby a more favorable entropy contribution would yield a higher selectivity at a higher temperature. As shown in Fig. 8, the O_2/N_2 selectivity through the bilayer membrane increases from 273 K to 300K, while it stays about the same for the single-layer membrane during the same temperature range.

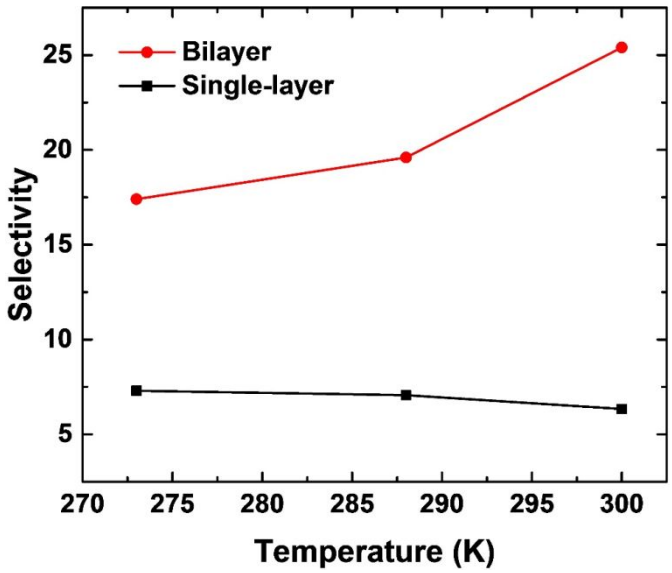

Fig. 8. Change of O_2/N_2 selectivity with temperature for single-layer and bilayer nanoporous graphene membranes.

3.5 Comparison of air-separation performances with available materials

Although our bilayer porous graphene membranes are still a design concept to be realized experimentally, it is still informative to compare with available materials in the literature for their air-separation performances, to show the distinctive features of the bilayer porous graphene membranes. As shown in Fig. 9, the bilayer porous graphene membranes have much higher permeances due to their sub-nanometer thickness, way beyond the upper bound.[16] More important, by harvesting the entropic selectivity via controlling the effective pore size, the bilayer porous graphene membranes can achieve higher O_2/N_2 selectivity, rivaling those of carbon-based mixed matrix membranes and carbon-molecular-sieve (CMS) membranes.

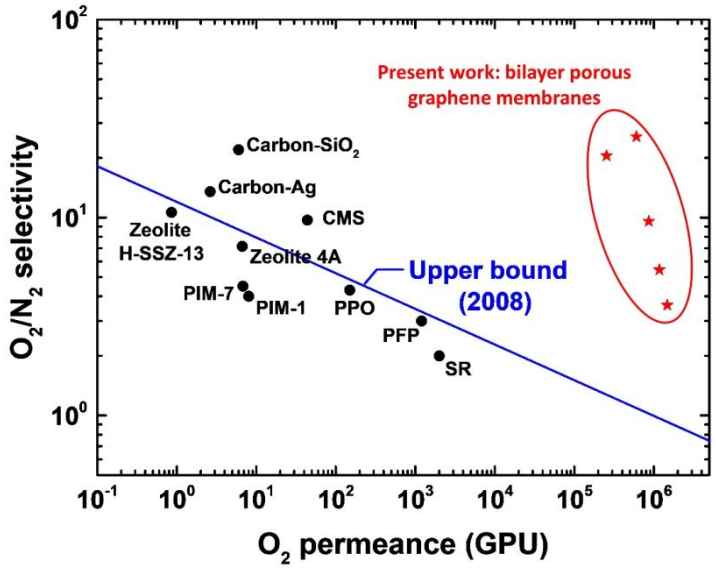

Fig. 9. Comparison of bilayer porous graphene membranes to other membranes for O_2/N_2 separation.[8, 38] The upper bound for polymer membranes is plotted with an assumed 1 μm-thick selective layer.[38] CMS: carbon molecular sieve; PPO: poly(phenylene oxide); PFP: perfluoropolymer; SR: silicone rubber.

The bilayer design is not limited to graphene membranes and could also be extended to 2D covalent-organic frameworks (COFs) and MOFs. To experimentally realize such design, we propose to first prepare a single-layer membrane with uniform pore sizes. There has been great progress recently in bottom-up synthesis of single-layer porous graphene.[39] More excitingly, 2D COFs[40] and MOFs[41, 42] have also been created by exfoliation. Once such a 2D membrane with uniform pores is available, one can stack such two layers together randomly to create the bilayer membranes with different offsets, or one can fold it into a bilayer, as experimentally demonstrated recently.[43]

4. CONCLUSIONS

In summary, we have demonstrated by classical molecular dynamics simulations that bilayer nanoporous graphene membranes with a proper effective pore size can achieve an O_2/N_2 selectivity as high as 26, while maintaining an O_2 permeance above 10^5 GPU. By tracking the trajectories of

gas-permeation events, we found that the high O_2/N_2 permselectivity is mainly contributed by the extra tumbling motion of O_2 molecules through the elliptical-shaped pore. Both transition-state theory analysis, simulated free-energy profiles, and temperature-dependent permeation confirm this entropic contribution to the selectivity. Our work hence shows that the bilayer nanoporous graphene membrane is effective for air separation and could be potentially useful for other separations by enhancing entropic selectivity.

Acknowledgements

This work was sponsored by the U.S. Department of Energy, Office of Science, Office of Basic Energy Sciences, Chemical Sciences, Geosciences, and Biosciences Division. This research used resources of the National Energy Research Scientific Computing Center, a DOE Office of Science User Facility supported by the Office of Science of the U.S. Department of Energy under Contract No. DE-AC02-05CH11231.

Electronic Supplementary Information

Pore size calculations; entropy estimate; force field parameters

Conflicts of interest

The authors declare no competing financial interests.

References

1 W. Castle, *Int. J. Refrig.*, 2002, **25**, 158-172.

2 T. Burdyny and H. Struchtrup, *Energy*, 2010, **35**, 1884-1897.

3 Y. Zhu, S. Legg and C. D. Laird, *Comput. Chem. Eng.*, 2010, **34**, 1377-1384.

4 R. S. Murali, T. Sankarshana and S. Sridhar, *Sep. Purif. Rev.*, 2013, **42**, 130-186.

5 A. Smith and J. Klosek, *Fuel Process. Technol.*, 2001, **70**, 115-134.

6 A. Singh-Ghosal and W. Koros, *J. Membr. Sci.*, 2000, **174**, 177-188.

7 R. W. Baker, *Ind. Eng. Chem. Res.*, 2002, **41**, 1393-1411.

8 P. Bernardo, E. Drioli and G. Golemme, *Ind. Eng. Chem. Res.*, 2009, **48**, 4638-4663.

9 W. F. Yong, F. Y. Li, Y. C. Xiao, T. S. Chung and Y. W. Tong, *J. Membr. Sci.*, 2013, **443**, 156-169.

10 A. Singh and W. Koros, *Ind. Eng. Chem. Res.*, 1996, **35**, 1231-1234.

11 C. Reid, I. O'koy and K. Thomas, *Langmuir*, 1998, **14**, 2415-2425.

12 R. P. Wesołowski and A. P. Terzyk, *Phys. Chem. Chem. Phys.*, 2016, **18**, 17018-17023.

13 C. Reid and K. Thomas, *Langmuir*, 1999, **15**, 3206-3218.

14 W. J. Koros and C. Zhang, *Nat. Mater.*, 2017, **16**, 289-297.

15 L. M. Robeson, *J. Membr. Sci.*, 1991, **62**, 165-185.

16 L. M. Robeson, *J. Membr. Sci.*, 2008, **320**, 390-400.

17 R. P. Wesołowski and A. P. Terzyk, *Phys. Chem. Chem. Phys.*, 2011, **13**, 17027-17029.

18 D.-e. Jiang, V. R. Cooper and S. Dai, *Nano Lett.*, 2009, **9**, 4019-4024.

19 Y. Jiao, A. Du, M. Hankel and S. C. Smith, *Phys. Chem. Chem. Phys.*, 2013, **15**, 4832-4843.

20 S. P. Koenig, L. Wang, J. Pellegrino and J. S. Bunch, *Nat. Nanotechnol.*, 2012, **7**, 728-732.

21 Q. Tang, Z. Zhou and Z. Chen, *Nanoscale*, 2013, **5**, 4541-4583.

22 H. Liu, S. Dai and D.-e. Jiang, *Nanoscale*, 2013, **5**, 9984-9987.

23 M. Dahanayaka, B. Liu, Z. Hu, Q.-X. Pei, Z. Chen, A. W.-K. Law and K. Zhou, *Phys. Chem. Chem. Phys.*, 2017, **19**, 30551-30561.

24 N. Raghav, S. Chakraborty and P. K. Maiti, *Phys. Chem. Chem. Phys.*, 2015, **17**, 20557-20562.

25 S. Plimpton, *J. Comput. Phys.*, 1995, **117**, 1-19.

26 S. Nosé, *J. Chem. Phys.*, 1984, **81**, 511-519.

27 W. G. Hoover, *Phys. Rev. A*, 1985, **31**, 1695-1697.

28 Y. Sun and S. Han, *Mol. Simulat.*, 2015, **41**, 1095-1109.

29 R. W. Hockney and J. W. Eastwood, *Computer simulation using particles*, CRC Press1988.

30 I.-C. Yeh and M. L. Berkowitz, *J. Chem. Phys.*, 1999, **111**, 3155-3162.

31 V. Ballenegger, A. Arnold and J. Cerda, *J. Chem. Phys.*, 2009, **131**, 094107.

32 M. Bonomi, D. Branduardi, G. Bussi, C. Camilloni, D. Provasi, P. Raiteri, D. Donadio, F. Marinelli, F. Pietrucci and R. A. Broglia, *Comput. Phys. Commun.*, 2009, **180**, 1961-1972.

33 S. Kumar, J. M. Rosenberg, D. Bouzida, R. H. Swendsen and P. A. Kollman, *J. Comput. Chem.*, 1995, **16**, 1339-1350.

34 S. Wang, S. Dai and D.-e. Jiang, *ACS Appl. Nano Mater.*, 2019, **2**, 379-384.

35 C. Sun and B. Bai, *J. Phys. Chem. C*, 2018, **122**, 6178-6185.

36 N. F. Himma, A. K. Wardani, N. Prasetya, P. T. Aryanti and I. G. Wenten, *Rev. Chem. Eng.*, 2018, **20170094**, 2191-0235.

37 C. Z. Sun, M. S. H. Boutilier, H. Au, P. Poesio, B. F. Bai, R. Karnik and N. G. Hadjiconstantinou, *Langmuir*, 2014, **30**, 675-682.

38 H. Lin, M. Zhou, J. Ly, J. Vu, J. G. Wijmans, T. C. Merkel, J. Jin, A. Haldeman, E. H. Wagener and D. Rue, *Ind. Eng. Chem. Res.*, 2013, **52**, 10820-10834.

39 C. Moreno, M. Vilas-Varela, B. Kretz, A. Garcia-Lekue, M. V. Costache, M. Paradinas, M. Panighel, G. Ceballos, S. O. Valenzuela and D. Peña, *Science*, 2018, **360**, 199-203.

40 Y. Peng, Y. Huang, Y. Zhu, B. Chen, L. Wang, Z. Lai, Z. Zhang, M. Zhao, C. Tan and N. Yang, *J. Am. Chem. Soc.*, 2017, **139**, 8698-8704.

41 Y. Peng, Y. Li, Y. Ban, H. Jin, W. Jiao, X. Liu and W. Yang, *Science*, 2014, **346**, 1356-1359.

42 Y. Peng, Y. Li, Y. Ban and W. Yang, *Angew. Chem. Int. Ed.*, 2017, **56**, 9757-9761.

43 B. Wang, M. Huang, N. Y. Kim, B. V. Cunning, Y. Huang, D. Qu, X. Chen, S. Jin, M. Biswal and X. Zhang, *Nano Lett.*, 2017, **17**, 1467-1473.